

RESEARCH ARTICLE

Life-cycle assessment for flutter probability of a long-span suspension bridge based on field monitoring data

Xiaolei Chu¹ | Hung Nguyen Sinh² | Wei Cui^{*1,3} | Lin Zhao^{1,3,4} | Yaojun Ge^{1,3}

¹State Key Lab of Disaster Reduction in Civil Engineering, Tongji University, Shanghai, China

²Amazon.com Inc., Seattle, WA, USA

³Key Laboratory of Transport Industry of Bridge Wind Resistance Technologies, Tongji University, Shanghai, China

⁴State Key Laboratory of Mountain Bridge and Tunnel Engineering, Chongqing Jiaotong University, Chongqing, China

Correspondence

*Wei Cui, 207 Wind Engineering Building, Tongji University, 1239 Siping Road, Shanghai, 200092, China. Email: cuiwei@tongji.edu.cn

Summary

Assessment of structural safety status is of paramount importance for existing bridges, where accurate evaluation of flutter probability is essential for long-span bridges. In current engineering practice, at the design stage, flutter critical wind speed is usually estimated by the wind tunnel test, which is sensitive to modal frequencies and damping ratios. After construction, structural properties of existing structures will change with time due to various factors, such as structural deteriorations and periodic environments. The structural dynamic properties, such as modal frequencies and damping ratios, cannot be considered as the same values as the initial ones, and the deteriorations should be included when estimating the life-cycle flutter probability. This paper proposes an evaluation framework to assess the life-cycle flutter probability of long-span bridges considering the deteriorations of structural properties, based on field monitoring data. The Bayesian approach is employed for modal identification of a suspension bridge with the main span of 1650 m, and the field monitoring data during 2010–2015 is analyzed to determine the deterioration functions of modal frequencies and damping ratios, as well as their inter-seasonal fluctuations. According to the historical trend, the long-term structural properties can be predicted, and the probability distributions of flutter critical wind speed for each year in the long term are calculated. Consequently, the life-cycle flutter probability is estimated, based on the predicted modal frequencies and damping ratios.

KEYWORDS:

long-span bridge, flutter probability, dynamic properties, Bayesian approach, field monitoring, life-cycle assessment

1 | INTRODUCTION

Flutter is a dynamic instability phenomenon of an elastic structure in the wind flow. In 1940, Tacoma Narrows Bridge collapsed four months after it was built, attracting the attention of flutter reliability. Severe consequences induced by flutter have motivated investigations for prediction of the flutter critical wind speed^{1,2} and for assessment of flutter probability^{3,4,5}. Furthermore, with the ever-growing increase of bridge span, assessment for aerodynamic performance becomes much more significant.

Modal frequencies and damping ratios are two important parameters for bridge flutter-resistance performance. In existing methods, the evaluation of flutter performance for long-span bridges has been comprehensively conducted by wind tunnel tests^{6,7} and numerical methods^{8,9}. However, the investigation of life-cycle flutter probability of in-service long-span bridges is very rare,

especially considering structural deteriorations of dynamic properties based on field monitoring data. In recent years, structural health monitoring (SHM) system, as an effective tool to record structural responses¹⁰, can provide sufficient structural vibration information and external excitation, and infer structural conditions¹¹. Based on these data, it is possible to analyze the structural dynamic properties and corresponding changing trends comprehensively, and predict their future performance consequently.

Practically, ambient vibration tests have attracted increasing attention in modal identification, which can be performed effectively onto structures in working conditions and without artificial intervention^{12,13,14}. Ambient modal identification, including the determination of modal frequencies, damping ratios, and mode shapes of a constructed structure using measured data¹⁵, does not require loading conditions in advance, but assume the external excitation is statistically random rather than constant. Stochastic subspace identification (SSI) method¹⁶ and Enhanced Frequency Domain Decomposition (EFDD) method¹⁷ in time domain are popular techniques capable of quickly extracting structural properties. Bayesian system identification approach^{18,19,20} is another popular method, viewing modal identification as an inference problem where probability is utilized as a measure for the plausibility of outcomes given a model of the system and measured data. The general principle of Bayesian identification is considering the objectives as a joint posterior probability density function (PDF) of the modal parameters for given measured data and modeling assumptions. In typical applications where there is a sufficiently large amount of data, the modal parameters are “globally identifiable” and the posterior PDF can be well approximated by a Gaussian PDF²¹, which is completely characterized by the most probable value (MPV) and the covariance matrix^{13,14,21}.

On the other hand, the assessment of flutter-resistance performance is an important research field for bridge engineering, considering the emerging trend of performance-based wind engineering^{22,23,24}. Current reliability evaluation methods for bridge flutter-resistance performance^{25,26,27} are based on multi-mode² and full-mode²⁸ approaches, and incorporate the effects of uncertainty either by numerical simulations²⁵ (e.g., Monte-Carlo sampling method) or by probability propagation methods^{29,30}. Recent studies in existing literatures have suggested that the flutter probability can be successfully assessed by the first-order reliability method (FORM)³¹, the “response surface method”³², the polynomial chaos expansion³³ and the artificial neural network model³⁴, etc.. Another method³⁵ has proposed the solution to the flutter probability problem by perturbation of the deterministic flutter velocity through a set of dimensionless multiplicative random parameters. Canor and Caracoglia³⁶ discussed the advantages and limitations of several reliability-based methods (e.g., random perturbation analysis, collocation methods, Galerkin approach). In this paper, a linear regression model is proposed to derive the PDF of flutter critical wind speed directly from the PDFs of modal frequencies and damping ratios. Long-span bridges are vulnerable to long-term environmental corrosion and fatigue damage accumulation, which is stochastic in nature and makes structural reliability time-variant. The challenges posed by aging structures have prompted several research programs to address risk management problems^{37,38,39}. Assessment procedures considering modification of structural properties can have a better insight into structural performances over extended time frames^{40,41}.

In this paper, an evaluation framework is proposed to assess life-cycle reliability of existing bridges in terms of flutter-resistance performance, based on field monitoring data. The historical trends are fitted to modify structural properties, utilizing monitoring data from 2010 to 2015. Furthermore, modal frequencies and damping ratios are sensitive to the in-service environment⁴², and the annual fluctuations of modal properties due to uncertain environmental factors are considered to obey time-invariant probability distributions fitted by field monitoring results. At last, probability distributions of flutter critical wind speed are calculated for each year, then the time-variant flutter probability is subsequently predicted.

2 | BACKGROUND METHODOLOGY

2.1 | Flutter critical wind speed

In multi-mode analysis, deflection components of the bridge deck are represented in terms of generalized coordinate $\xi_i(t_s)$, deck width B , and dimensionless modal values of the i -th mode along the deck $h_i(x)$, $p_i(x)$, and $\alpha_i(x)$, as shown in Fig. 1.

Bridge aeroelastic forces can be simplified by exclusively considering the vertical force (L_{ae}) and torsional moment (M_{ae}) per unit deck span⁴³, which are expressed by

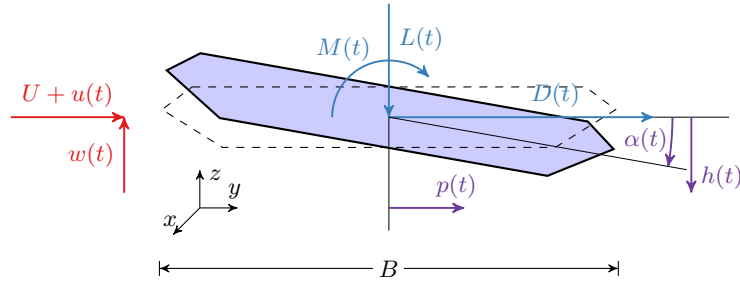


FIGURE 1 Bridge section and coordinate definition

$$L_{ae}(x, t_s) = \frac{\rho U^2 B}{2} \left[\frac{K H_1^* \dot{h}(x, t_s)/U + K H_2^* B \dot{\alpha}(x, t_s)/U +}{K^2 H_3^* \alpha(x, t_s) + K^2 H_4^* h(x, t_s)/B} \right] \quad (1a)$$

$$M_{ae}(x, t_s) = \frac{\rho U^2 B^2}{2} \left[\frac{K A_1^* h(x, t_s)/U + K A_2^* B \dot{\alpha}(x, t_s)/U +}{K^2 A_3^* \alpha(x, t_s) + K^2 A_4^* h(x, t_s)/B} \right], \quad (1b)$$

where B is the deck width; U is the mean wind velocity at the deck level, acting orthogonally to the longitudinal axis; ρ is the air density; t_s is the time variable, unit of which is second; $K = \omega B/U$ is the reduced frequency; $\dot{h}(t_s) = dh/dt_s$ and $\dot{\alpha}(t_s) = d\alpha/dt_s$. By modal superpositions, the dynamic response in Fig. 1 of can be expressed as

$$h(x, t_s) = \sum_g h_g(x) B \xi_g(t_s) \quad (2a)$$

$$\alpha(x, t_s) = \sum_g \alpha_g(x) \xi_g(t_s) \quad (2b)$$

where x is the coordinate along the deck span; t_s is the time; $h_g(x)$ and $\alpha_g(x)$ are the dimensionless g -th mode shapes; $\xi_g(t_s)$ are associated generalized coordinates.

A coupled-two-mode system of dynamic equations can be further simplified by the first vertical mode and first torsional one as "v1" and "t1" with circular frequencies ω_v and ω_{t1} . The corresponding expressions are also simplified as uncoupled mode shapes $h_{v1}(x)$ and $\alpha_{t1}(x)$, respectively. Then Eq. (2) can be simplified as

$$h(x, t_s) \cong \xi_{v1}(t_s) B h_{v1}(x) \quad (3a)$$

$$\alpha(x, t_s) \cong \xi_{t1}(t_s) \alpha_{t1}(x) \quad (3b)$$

The coupled-mode aeroelastic instability can be derived⁴⁴ by Fourier-domain analysis of two-dimensional system of equations described above in terms of complex amplitudes of the generalized ξ_{v1} , ξ_{t1} in Eq. (3), expressed in vector form as $\bar{\xi} = [\bar{\xi}_{v1}, \bar{\xi}_{t1}]^T$. On-going flutter can be determined after representing the simple harmonic motion for both modes in terms of a critical reduced frequency ratio $\chi = K/K_{t1}$ ⁴⁴. The problem can be reduced to the nontrivial solutions of a two-by-two complex algebraic system $\mathbf{E}(K, \chi) \bar{\xi} = \mathbf{0}$ with $q_{v1} = 0.5\rho B^4 \ell / I_{v1}$ and $q_{t1} = 0.5\rho B^4 \ell / I_{t1}$. The scalar components of $\mathbf{E}(K, \chi)$ with $\mathbf{i} = \sqrt{-1}$ are

$$E_{1,1}(K, \chi) = \begin{bmatrix} -\chi^2 + (K_{v1}/K_{t1})^2 - q_{v1} \chi^2 H_4^*(K) G_{v1,v1} \\ +\mathbf{i} (2\zeta_{v1} K_{v1}/K_{t1} \chi - q_{v1} \chi^2 H_1^*(K) G_{v1,v1}) \end{bmatrix} \quad (4a)$$

$$E_{1,2}(K, \chi) = -q_{v1} (\chi^2 H_3^*(K) G_{v1,t1} + \mathbf{i} \chi^2 H_2^*(K) G_{v1,t1}) \quad (4b)$$

$$E_{2,1}(K, \chi) = -q_{v1} (\chi^2 A_4^*(K) G_{v1,t1} + \mathbf{i} \chi^2 A_1^*(K) G_{v1,t1}) \quad (4c)$$

$$E_{2,2}(K, \chi) = \begin{bmatrix} \chi^2 + 1 - q_{t1} \chi^2 A_3^*(K) G_{t1,t} \\ +\mathbf{i} (2\zeta_{t1} \chi - q_{t1} \chi^2 A_2^*(K) G_{t1,t1}) \end{bmatrix} \quad (4d)$$

where ζ_{v1} and ζ_{t1} are modal damping ratios; the reduced frequencies of the modes are $K_{v1} = \omega_{v1} B/U$ and $K_{t1} = \omega_{t1} B/U$. The dimensionless modal integrals⁴⁴ in Eq. (4) are : $G_{v1,v1} = \int_0^\ell h_{v1}^2(x) dx/\ell$, $G_{t1,t1} = \int_0^\ell \alpha_{t1}^2(x) dx/\ell$ and $G_{v1,t1} = \int_0^\ell h_{v1}(x) \alpha_{t1}(x) dx/\ell$ with ℓ being the longitudinal length of the bridge. Generalized modal inertias are $I_{v1} = m_0 \ell B^2 G_{v1,v1}$ and

$I_{t1} = I_0 \ell G_{t1,t1}$, with m_0 and I_0 being an equivalent mass and a mass moment of inertia perunit length of the moving structure. An iterative procedure is needed to solve for $\det[\mathbf{E}(K, \chi)] = 0$ ⁴⁴.

2.2 | Bayesian FFT Modal Identification

Yuen, Katafygiotis⁴⁵ and Au et al.^{13,14} developed an efficient algorithm to identify most probable values (MPV) and corresponding covariances of modal properties (e.g., modal frequencies and damping ratios) with well-separated modes and possibly close-spaced modes⁴⁶. The definitions of some quantities in this section have been adapted from the original formulation of Au¹³. If the acceleration time history measured at n DOFs of a structure is noted as $\{\hat{\mathbf{x}}_j \in \mathbb{R}^n : j = 1, \dots, N\}$ and abbreviated as $\{\hat{\mathbf{x}}_j\}$, where N = number of samples per channel, the FFT of $\{\hat{\mathbf{x}}_j\}$ is defined as

$$\mathcal{F}_k = \mathbf{F}_k + \mathbf{i}\mathbf{G}_k = \sqrt{(2\Delta t)/N} \sum_{j=1}^N \hat{\mathbf{x}}_j \exp\{-2\pi\mathbf{i}[(k-1)(j-1)/N]\} \quad (k = 1, \dots, N) \quad (5)$$

where $\mathbf{i}^2 = -1$; Δt is the sampling interval; $\mathbf{F}_k = \text{Re } \mathcal{F}_k$ and $\mathbf{G}_k = \text{Im } \mathcal{F}_k$ denote the real and imaginary part of the FFT, respectively. For $k = 2, 3, \dots, N_q$, the FFT corresponds to frequency $f_k = (k-1)/N\Delta t$. Here, $N_q = \text{int}[N/2] + 1$ ($\text{int}[\cdot]$ denotes the integer part) corresponds to the FFT ordinate at the Nyquist frequency. For modal identification only these $(N_q - 1)$ FFT values are utilized.

In the context of Bayesian inference, the measured acceleration is modeled as $\hat{\mathbf{x}}_j = \mathbf{x}_j(\boldsymbol{\theta}) + \boldsymbol{\epsilon}_j$ where $\mathbf{x}_j(\boldsymbol{\theta})$ is the acceleration response of the structural model defined by the set of model parameters $\boldsymbol{\theta}$, the subject to be identified; $\boldsymbol{\epsilon}_j$ is the prediction error that accounts for the deviation between the model response and measured data, possibly owing to measurement noise and modeling error. Yuen and Katafygiotis derived the joint PDF for the augmented FFT vectors $\{\mathbf{Z}_k = [\mathbf{F}_k^T, \mathbf{G}_k^T]^T \in \mathbb{R}^{2n} : k = 2, \dots, N_q\}$ and applied it to Bayesian modal identification⁴⁵. For a high sampling rate and long duration of data, \mathbf{Z}_k is a zero-mean Gaussian vector with covariance matrix given by

$$\mathbf{C}_k = \frac{1}{2} \begin{bmatrix} \boldsymbol{\Phi}(\text{Re } \mathbf{H}_k) \boldsymbol{\Phi}^T & -\boldsymbol{\Phi}(\text{Im } \mathbf{H}_k) \boldsymbol{\Phi}^T \\ \boldsymbol{\Phi}(\text{Im } \mathbf{H}_k) \boldsymbol{\Phi}^T & \boldsymbol{\Phi}(\text{Re } \mathbf{H}_k) \boldsymbol{\Phi}^T \end{bmatrix} + (\sigma^2/2) \mathbf{I}_{2n} \quad (6)$$

where $\boldsymbol{\Phi} \in \mathbb{R}^{n \times m}$ is the mode shape matrix confined to the measured DOFs (the i th column gives the i th mode shape); σ^2 is the (constant) spectral density level of the prediction error; \mathbf{I}_{2n} denotes the $2n \times 2n$ identity matrix; \mathbf{H}_k is the spectral density matrix of the model response and its (i, j) entry is given by

$$\mathbf{H}_k(i, j) = S_{ij} [(\beta_{ik}^2 - 1) + \mathbf{i}(2\zeta_i \beta_{ik})]^{-1} [(\beta_{jk}^2 - 1) - \mathbf{i}(2\zeta_j \beta_{jk})]^{-1} \quad (7)$$

where $\beta_{ik} = f^{(i)}/f_k$ = frequency ratio; $f^{(i)}$ and ζ_i = natural frequency and damping ratio of the i th mode, respectively; S_{ij} = cross spectral density between the i th and j th modal excitation.

The set of modal parameters $\boldsymbol{\theta}$ consists of modal frequencies, damping ratios, mode shapes, entries $\{\mathbf{S}_{ij}\}$ of the spectral density matrix of modal excitations and spectral density σ^2 of the prediction error. Assuming a noninformative prior distribution, the posterior PDF of $\boldsymbol{\theta}$ given the FFT data is proportional to the likelihood function $p(\{\mathbf{Z}_k\}|\boldsymbol{\theta})$

$$\begin{aligned} p(\boldsymbol{\theta}|\{\mathbf{Z}_k\}) &\propto p(\{\mathbf{Z}_k\}|\boldsymbol{\theta}) = (2\pi)^{-(N_q-1)/2} \left[\prod_{k=2}^{N_q} \det \mathbf{C}_k(\boldsymbol{\theta}) \right]^{-1/2} \\ &\times \exp \left[-(1/2) \sum_{k=2}^{N_q} \mathbf{Z}_k^T \mathbf{C}_k(\boldsymbol{\theta})^{-1} \mathbf{Z}_k \right] \end{aligned} \quad (8)$$

where the dependence of \mathbf{C}_k on $\boldsymbol{\theta}$ has been emphasized²¹. It is convenient to write with the negative log-likelihood function $L(\boldsymbol{\theta})$ form

$$p(\boldsymbol{\theta}|\{\mathbf{Z}_k\}) \propto \exp[-L(\boldsymbol{\theta})] \quad (9)$$

where

$$\begin{aligned} L(\boldsymbol{\theta}) &= (1/2) \sum_{k=2}^{N_q} [\ln \det \mathbf{C}_k(\boldsymbol{\theta}) + \mathbf{Z}_k^T \mathbf{C}_k(\boldsymbol{\theta})^{-1} \mathbf{Z}_k] \\ &\approx L(\hat{\boldsymbol{\theta}}) + \frac{1}{2}(\boldsymbol{\theta} - \hat{\boldsymbol{\theta}})^T H_L(\hat{\boldsymbol{\theta}})(\boldsymbol{\theta} - \hat{\boldsymbol{\theta}}) \end{aligned} \quad (10)$$

where the first-order term vanishes owing to optimality of $\hat{\theta}$; $H_L(\hat{\theta})$ is the Hessian of L at MPV (most probable value)^{13,14}. Substituting into Eq. (9), the posterior PDF becomes a Gaussian PDF

$$p(\theta | \{\mathbf{Z}_k\}) \propto \exp \left[-(1/2)(\theta - \hat{\theta})^T \hat{\mathbf{C}}^{-1} (\theta - \hat{\theta}) \right] \quad (11)$$

where

$$\hat{\mathbf{C}} = H_L(\hat{\theta})^{-1} \quad (12)$$

is the posterior covariance matrix.

MPVs of modal properties can be determined by minimizing $L(\theta)$. Practically, computational problems are inevitable while identifying mode shapes due to the large number of measured DOFs and calculating the inverse of the covariance matrix \mathbf{C}_k , which have been well explained and solved in^{13,14,47}.

2.3 | Life-cycle assessment of flutter reliability

Long-span bridges are susceptible to aging from various environmental or non-environmental factors, such as chemical attack, corrosion, climate change and other physical mechanisms^{40,41}. Age-related deterioration leads to a decrease of structural capacity to withstand various challenges during its service life from operating conditions, natural environments, and accidents^{48,40}, which makes life-cycle assessment necessary. Life-cycle assessment of long-span bridges ought to take possible deteriorations into accounts. SHM system offers a chance to monitor structural long-term structural properties, then corresponding changing trends can be found.

As for flutter-resistance performance, factors that affect the flutter stability can be summarized into two aspects, structural flutter-resistance ability V_R (i.e., flutter critical wind speed) and wind load effect V_S (i.e., site wind speed). In flutter analysis, V_R is the function of modal frequencies \mathbf{f} , damping ratios $\boldsymbol{\zeta}$ and flutter derivatives \mathbf{A}^* ($A_1^*, A_2^*, A_3^*, A_4^*$), \mathbf{H}^* ($H_1^*, H_2^*, H_3^*, H_4^*$). Structural properties will be time-variant due to aging and environmental factors. Based on field monitoring, changing trends of modal frequencies and damping ratios can be investigated. V_S is the site wind speed, which is normally described as extreme wind speeds distribution for certain time duration. For example, in the wind load design standard⁴⁹, Gumbel distribution is used to model annual extreme wind speeds. Based on V_R and V_S , a state function Z can be defined

$$Z(V_R, V_S; t) = V_R(\mathbf{f}(t), \boldsymbol{\zeta}(t), \mathbf{A}^*, \mathbf{H}^*) - V_S(t) \quad (13)$$

where $Z > 0$ denotes structural safety, $Z = 0$ denotes limit state and $Z < 0$ denotes structural failure; t is the time variable, unit of which is year.

In this research, $\mathbf{f}(t)$ and $\boldsymbol{\zeta}(t)$ are time-variant modal frequencies and damping ratios, respectively, fitted by field monitoring data; \mathbf{A}^* and \mathbf{H}^* are flutter derivatives, which are obtained by wind tunnel test and are functions of reduced velocities; $V_S(t)$ is the time-variant site wind speed. In reliability analysis, normal distribution is usually regarded as the most widely-used and accepted distribution for flutter derivatives considering its flexibility and simplicity²⁹. In this paper, the uncertainties of flutter derivatives are ignored because they are mainly caused by experimental error, and deteriorations due to aging are mainly concerned issues here. On the other hand, $V_S(t)$ is a time-variant variable susceptible to climate change, as preliminarily examined in^{25,50}. In this research, $V_S(t)$ is temporarily regarded to obey a constant Gumbel distribution, and its relationship with climate change remains to be investigated in the future. The PDFs of V_R and V_S are denoted as $f_R(r; t)$ and $f_S(s)$, respectively. Thus the structural failure (flutter on-site) probability⁵¹ is

$$\begin{aligned} P_f(t) &= P(Z \leq 0; t) = P(V_R(t) - V_S \leq 0) = \int \int_{r \leq s} f_{RS}(r, s; t) dr ds \\ &= \int \int_{r \leq s} f_R(r; t) \cdot f_S(s) dr ds = \int_{-\infty}^{+\infty} \left[\int_{-\infty}^s f_R(r; t) dr \right] \cdot f_S(s) ds \end{aligned} \quad (14)$$

Ge and Tanaka²⁸ elaborated the difference with various number of selected natural modes participating in the flutter by multi-mode flutter analysis, showing that the error between two modes (fundamental vertical mode and torsional mode) and multiple modes (up to 7 modes included) is less than 0.3%. As a result, two modes (fundamental vertical and torsional modes) are accurate to calculate the flutter critical wind speed. In this paper, only 1st-order asymmetric vertical mode and 1st-order asymmetric

torsional mode are considered in the calculation of the flutter critical wind speed. In order to clarify how randomness is delivered from structural properties to the flutter critical wind speed, a linear regression model is proposed as Eq. (15)

$$V_R = \alpha_{v1} f_{v1} + \alpha_{t1} f_{t1} + \beta_{v1} \zeta_{v1} + \beta_{t1} \zeta_{t1} + c \quad (15)$$

where α_{v1} , α_{t1} , β_{v1} and β_{t1} are regression coefficients; c is constant; f_{v1} , ζ_{v1} and f_{t1} , ζ_{t1} are modal frequencies and damping ratios, respectively for 1st-order vertical mode and 1st-order torsional mode.

If the variances of f_i and ζ_i ($i = v1, t1$) in Eq. (15) are independent (as shown in Fig. 13), the PDF $f_R(r)$ of the flutter critical wind speed can be directly obtained from the structural properties' PDFs

$$f_R(r) = \frac{1}{|\alpha_{v1} \alpha_{t1} \beta_{v1} \beta_{t1}|} \int \int \int_{-\infty}^{+\infty} f_{f,v1} \left(\frac{x_1}{\alpha_{v1}} \right) f_{f,t1} \left(\frac{x_2 - x_1}{\alpha_{t1}} \right) f_{\zeta,v1} \left(\frac{x_3 - x_2}{\beta_{v1}} \right) f_{\zeta,t1} \left(\frac{r - x_3 - c}{\beta_{t1}} \right) dx_1 dx_2 dx_3 \quad (16)$$

where $f_{f,i}(\cdot)$ ($i = v1, t1$) denote PDFs of modal frequencies; $f_{\zeta,i}(\cdot)$ ($i = v1, t1$) denote PDFs of damping ratios.

3 | ASSESSMENT FRAMEWORK

The evaluation of flutter probability is a well-known issue. In this paper, a linear regression model is proposed to predict the PDF of flutter critical wind speed given that the PDFs of structural properties are known. Then the probability interference method is utilized to evaluate the life-cycle flutter probability. The whole process can be summarized as the following procedure.

1. Structural vibration data is collected from the health monitoring system, and Bayesian FFT modal identification is carried out to obtain structural properties, including modal frequencies and damping ratios. Futuristic evolving trends of structural properties are predicted, as well as their probability distributions.
2. Meteorological data is processed at the structure site to evaluate the PDF of annual wind speed.
3. Obtain flutter derivatives by wind tunnel test.
4. Estimate time-variant PDFs of structural properties to get the PDF of the flutter critical wind speed for each year by the proposed linear regression model, then assess long-term bridge reliability in terms of flutter probability.

The whole framework is illustrated in Fig. 2.

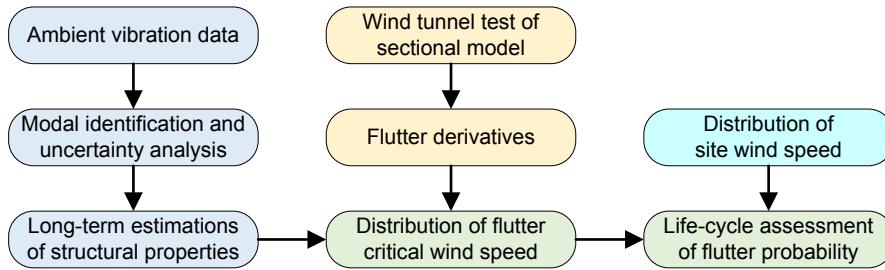


FIGURE 2 Flow chart of assessment of flutter probability

4 | APPLICATION EXAMPLE

4.1 | Description of the bridge example

To demonstrate the feasibility of the proposed framework, this study utilizes field monitoring data from Xihoumen Bridge during 2010-2015. As shown in Fig. 3, Xihoumen Bridge is a suspension bridge with a 1650-meter central main span linking Jintang and Cezi islands near the East China Sea coast. In its health monitoring system, UA1-UA6 are ultrasonic anemometers (UAs);

AC10-AC18 are servo accelerometers (ACs). The sampling rate of the UAs is 32Hz, and the measuring range is 0-65m/s. UAs can record wind speeds for 3 directions simultaneously: north, west, and upward (vertical). The sampling rate of the ACs is 100Hz in 2010 and 2011, 50Hz in 2012-2015. ACs can record accelerations of vertical and lateral directions of the bridge cross section. The detailed information of UAs and ACs is presented in Tab. 1 and Fig. 3.

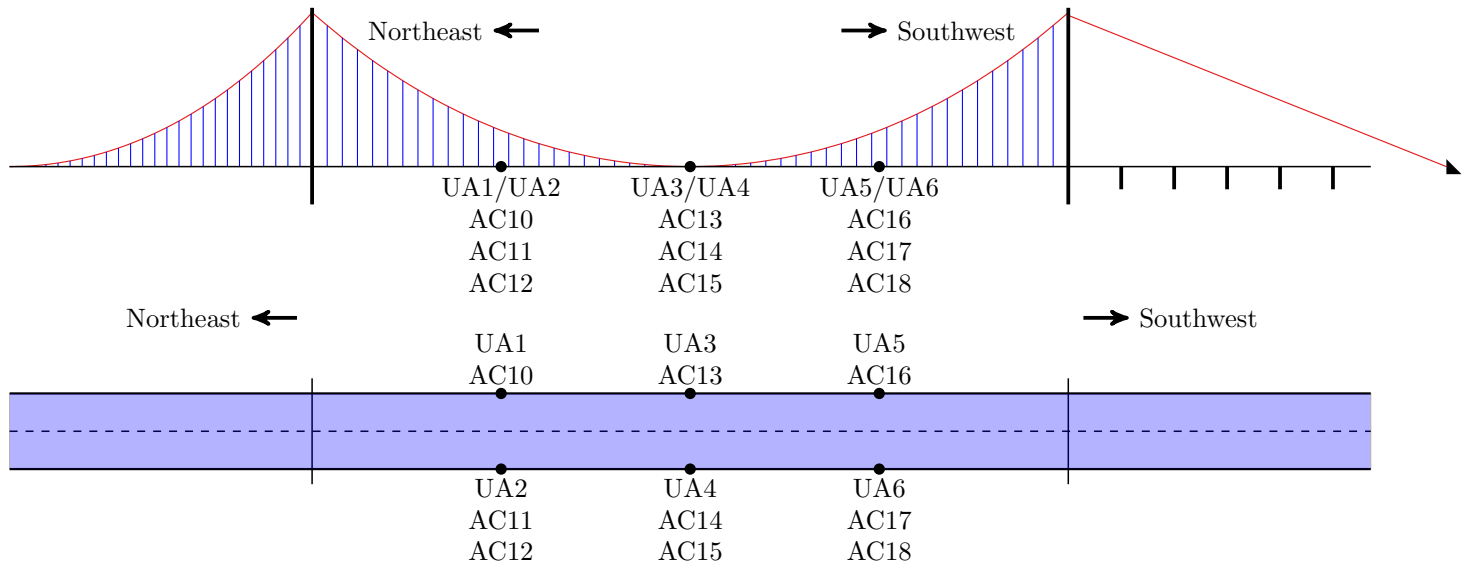


FIGURE 3 Elevation of Xihoumen Bridge and layout of monitoring points

TABLE 1 Definition of sensors

Sensor number	Sensor type	Location
UA1/UA2	ultrasonic anemometer	main span (1/4)
UA3/UA4	ultrasonic anemometer	main span (1/2)
UA5/UA6	ultrasonic anemometer	main span (3/4)
AC10/AC11/AC12	servo accelerometer	main span 1/4 (vertical/lateral/vertical)
AC13/AC14/AC15	servo accelerometer	main span 1/2 (vertical/lateral/vertical)
AC16/AC17/AC18	servo accelerometer	main span 3/4 (vertical/lateral/vertical)

In this study, the authors utilize vertical responses at two sides of the bridge deck (i.e., AC10, AC12, AC13, AC15, AC16, AC18) because flutter usually occurs as coupled vertical and torsional motions. The acceleration histories (six years in total) are analyzed by hour. Furthermore, the authors utilize hourly-averaged wind speeds at the middle span (UA4) as a filter to reduce identification errors. In this study, only acceleration responses with hourly-averaged wind speeds of 2-4 m/s are adopted to avoid possible vortex-induced lock-in phenomenon (as examined by Li et al.⁵², 6-10 m/s). The reason is that when the vortex-induced vibration occurs, the bridge will be characterized by single vibration mode, which is against the assumption of fast Bayesian approach that the ambient excitation is statistically random, instead of a single fixed frequency. 2-4 m/s is an appropriate range of speeds, since it not only provides sufficient external excitations, but also avoids excessive aeroelastic effects during buffeting excitation. Moreover, in order to avoid the deviation caused by possible heavy traffic flow, only monitoring data during 0 am - 7 am is adopted.

4.2 | Bayesian FFT modal identification results

The structural properties are significant for assessment of bridge flutter-resistance performance. The fast Bayesian approach is a useful method for modal identification of long-span bridges⁴⁶ for the output-only system under ambient excitations⁴⁵.

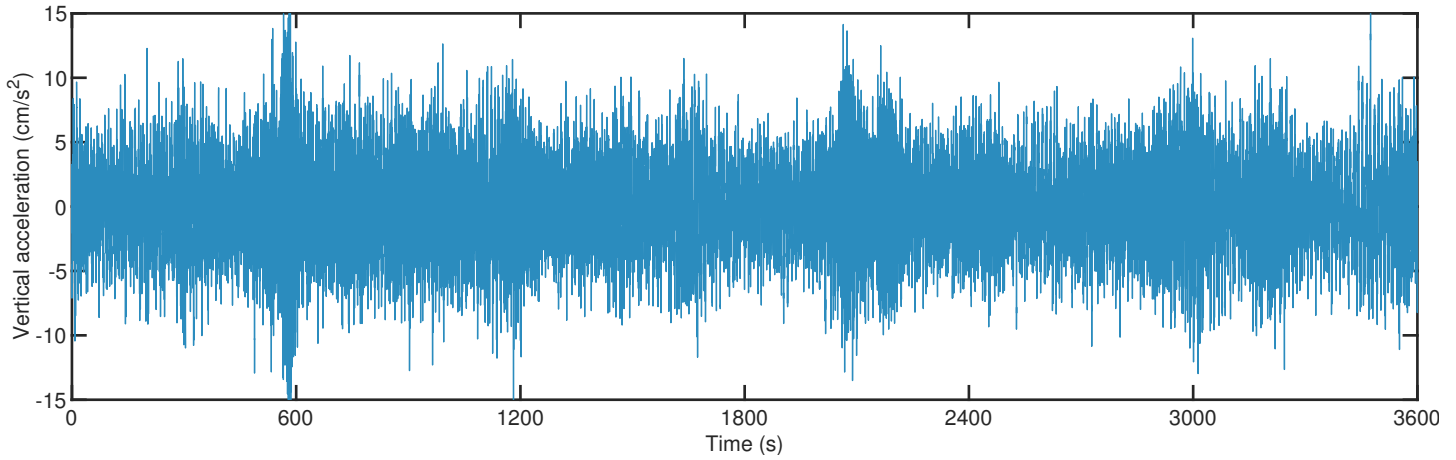


FIGURE 4 Time history of one-hour vertical accelerations

A representative segment of measured vertical acceleration is shown in Fig. 4. The results analyzed by SSI method^{52,53} and EFDD method⁵³ have been implemented by some researchers. Li et al.⁵² investigated the vortex-induced vibration and structural properties (modal frequencies and damping ratios) of Xihoumen Bridge based on SSI method. Yang et al.⁵³ carried out the ambient vibration test of Xihoumen Bridge under conditions that the wind speed during the test ranged from 2m/s to 8m/s, and identify structural properties based on SSI method and EFDD method⁵³. Tab. 2 shows results identified by fast Bayesian approach, as well as the results from EFDD method and SSI method for comparison. Tab. 2 shows that frequencies identified by different methods have a high consistency. However, there exists large discrepancies in damping ratios. The damping ratios identified by Bayesian approach are usually smaller, compared with SSI method and EFDD method. Zhang et al.⁵⁴ also found a similar regularity that the damping ratios obtained by Bayesian approach are relatively smaller than those obtained by SSI method and EFDD method when they launched the operational modal analysis of a 250m super-tall building. This might be caused by different mechanisms while identifying damping ratios with different methods, as explained by Zhang et al.⁵⁴. On the other hand, different ambient conditions (e.g., temperature, humidity, wind, etc.) also make a significant difference to damping ratios^{55,56}. Therefore, the discrepancies shown in damping ratios are reasonable, since the field monitoring data, utilized for identification by Li et al.⁵², Yang et al.⁵³ and this study, are under fairly different ambient environments (with different temperature, humidity and so on). What's more, similar with many researchers' results^{46,54} (identified by the Bayesian approach), the Bayesian coefficients of variance (COV) (=posterior standard deviation/MPV, as mentioned in Tab. 2) of damping ratios are much more remarkable than those of modal frequencies. This also indicates that the changeable ambient environment influences the identified damping ratios greatly.

Fig. 5 presents the identified modal frequencies and damping ratios by fast Bayesian approach during 2010-2015, where the vibration data is hourly-segmented for analysis. The MPV (most probable value) is denoted by red lines. The blue area denotes the range of $MPV \pm$ posterior standard deviation ($MPV \pm \sigma$), which indicates measurement errors. The variances of structural properties' MPVs show an obvious inter-seasonal fluctuating characteristic, which may be influenced by the periodic variances of environmental factors, such as temperature, humidity, etc..

For modal frequencies, they are directly associated with structural stiffness, because if the mass M is assumed as constant, then a deterioration of stiffness K leads to a decrease of modal frequencies ($f \propto \sqrt{K/M} \propto \sqrt{K}$). Combined with the periodic environment, modal frequencies are believed to decline generally and fluctuate inter-seasonally, as examined by Yuen et al.⁵⁷. The long-term variation of damping ratios is more complicated, related with various factors^{55,56}. Its long-term trend could be determined by health monitoring data. Similarly with modal frequencies, damping ratios also fluctuate inter-seasonally with the periodic environment.

TABLE 2 The measured modal frequencies and damping ratios from vertical vibration by EFDD method⁵³, SSI method^{52,53} and fast Bayesian approach

EFDD/SSI Method ⁵³	Frequency(Hz)			EFDD Method ⁵³	SSI Method ⁵³	Damping Ratio(%)			Mode Shape
	SSI Method ⁵²	Bayesian Method	Bayesian Frequency COV (σ /MPV)			SSI Method ⁵²	Bayesian Method	Bayesian Damping Ratio COV (σ /MPV)	
0.095	0.0953	0.0948	0.2279%	1.12~2.64	1.80~2.18	0.57	0.78	32.48%	1-AS-V
0.133	0.1328	0.1330	0.1080%	0.84~2.32	0.90~1.46	0.52	0.47	32.57%	2-S-V
0.183	0.1825	0.1828	0.0547%	0.18~1.02	0.37~0.61	0.50	0.32	32.15%	2-AS-V
0.229	0.2301	0.2302	0.0963%	0.21~0.59	0.23~0.62	0.51	0.29	37.54%	1-S-T
0.233	\	0.2383	0.0801%	0.25~0.41	0.77~0.95	\	0.31	44.55%	1-AS-T
0.276	0.2767	0.2767	0.0820%	0.34~1.14	0.43~0.83	0.39	0.30	26.99%	3-AS-V

¹ Note: S-symmetric, AS-asymmetric, V-vertical bending, T-torsion

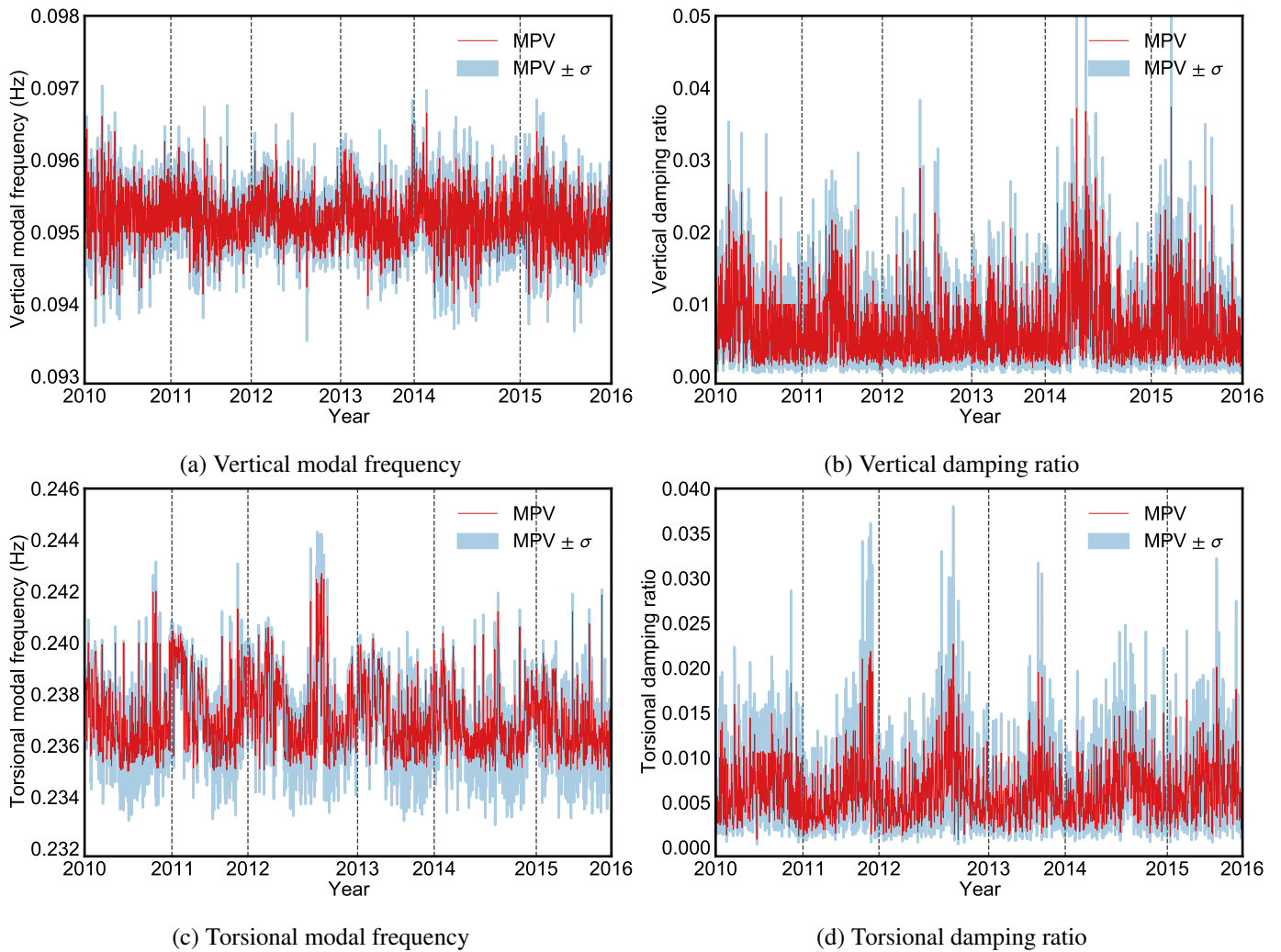


FIGURE 5 1st-order asymmetric vertical and torsional modes: modal frequencies and damping ratios identified by fast Bayesian approach

In order to delineate long-term trends and inter-seasonal fluctuations of structural properties more clearly, historical data from SHM system is of much significance. In Sec. 5, identified long-term MPVs are utilized to fit the long-term trends and model the inter-seasonal fluctuations by probability distributions.

4.3 | Design wind speed at bridge site

Xihoumen Bridge is a cross-sea bridge located at Zhoushan City, often invaded by typhoons⁵⁸. According to the wind-resistance design specification⁴⁹, wind velocities of all directional magnitudes at the deck height with 10-year, 50-year and 100-year return periods can be obtained, respectively 35.64 m/s, 46.48 m/s and 50.47 m/s. The Gumbel distribution⁴⁹ is utilized to fit the annual wind velocity. The probability density function (PDF) of Gumbel distribution with location parameter μ and scale parameter σ is

$$f(s|\mu, \sigma) = \sigma^{-1} \exp\left(-\left(\frac{s-\mu}{\sigma} + \exp\left(-\left(\frac{s-\mu}{\sigma}\right)\right)\right)\right) \quad (17)$$

By Eq. (17), it can be deduced $\mu = 24.1973$ and $\sigma = 5.7115$. The distribution of site wind at Xihoumen Bridge is depicted in Fig. 6.

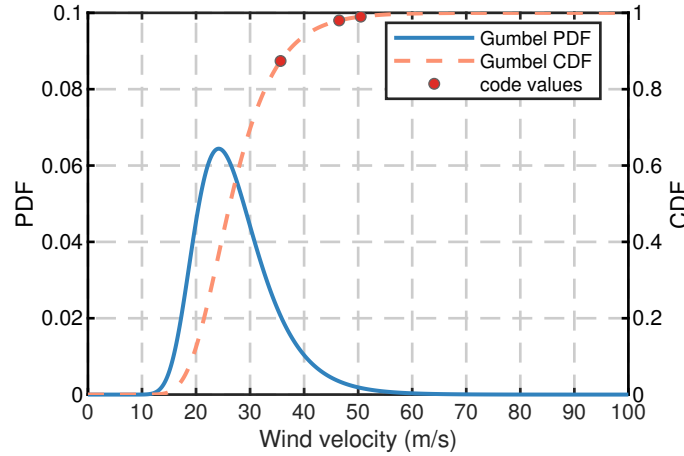


FIGURE 6 Probability distribution of site wind at Xihoumen Bridge

4.4 | Flutter derivatives

The detailed experimental set-up information can be found in the wind tunnel test by Yang et al.⁵³. Fig. 7 presents the identified flutter derivatives. All flutter derivatives are fitted by quadratic polynomial except H_2^* , which is fitted by quartic polynomial. As examined by Li et al.⁵², vortex-induced vibration would occur at a low wind velocity (6-10 m/s). Therefore, there will exist aberrant values at certain low reduced velocities in Fig. 7(d), Fig. 7(e) and Fig. 7(h), where the abnormal points are excluded in order to improve the fitting accuracy. It is reasonable because in this application example, the reduced velocity will range from 8 to 13 when the bridge flutter occurs.

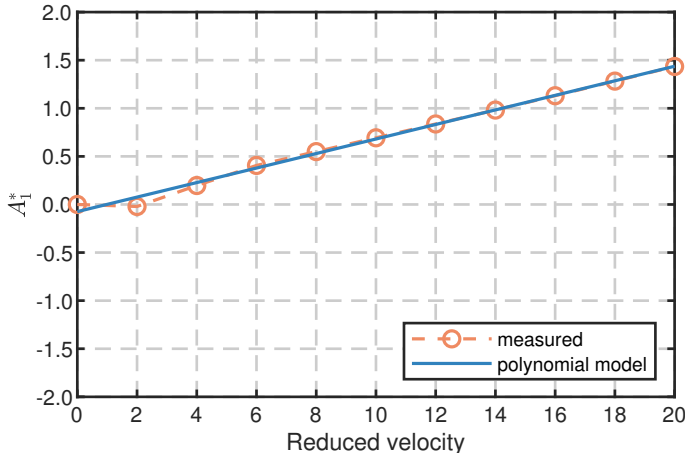
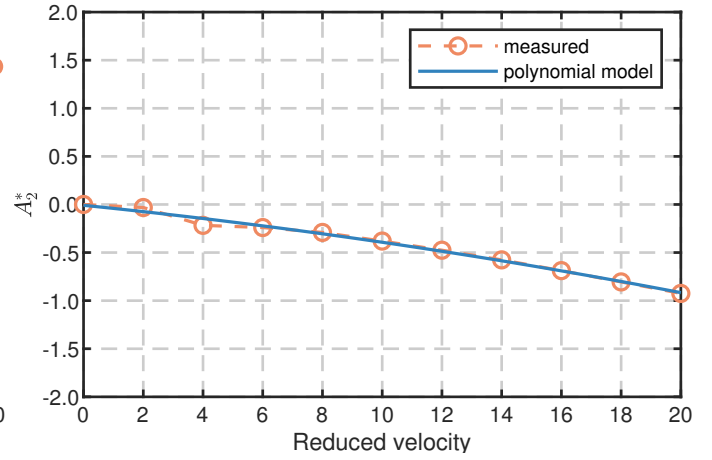
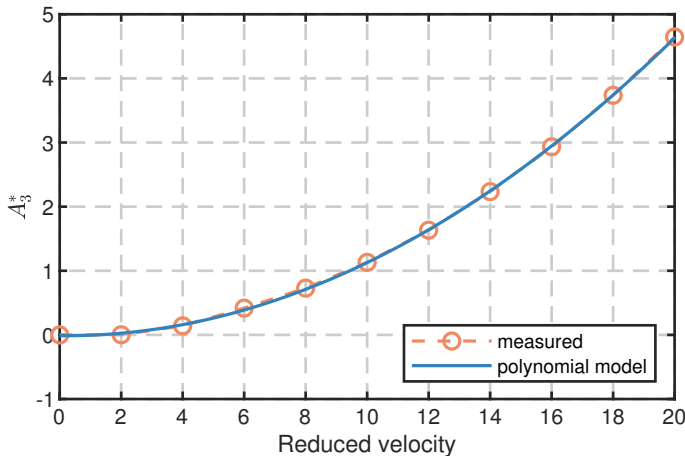
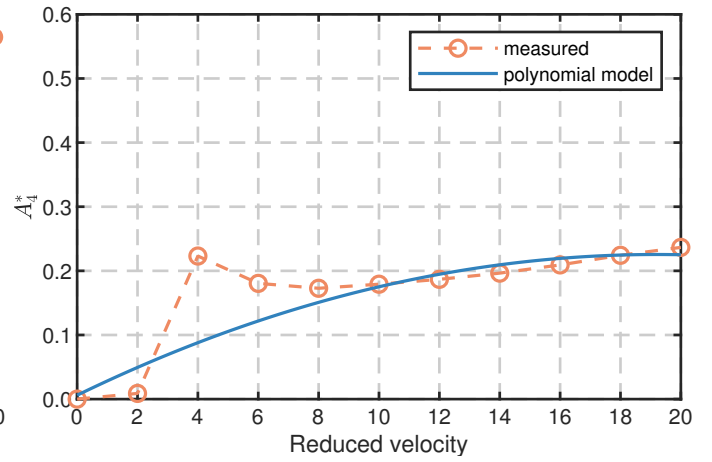
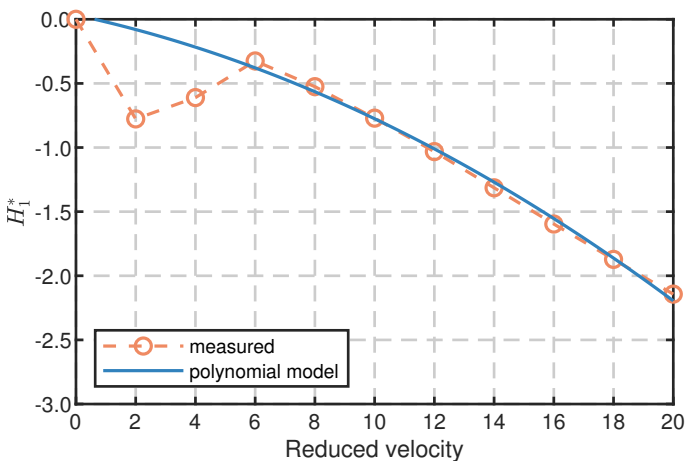
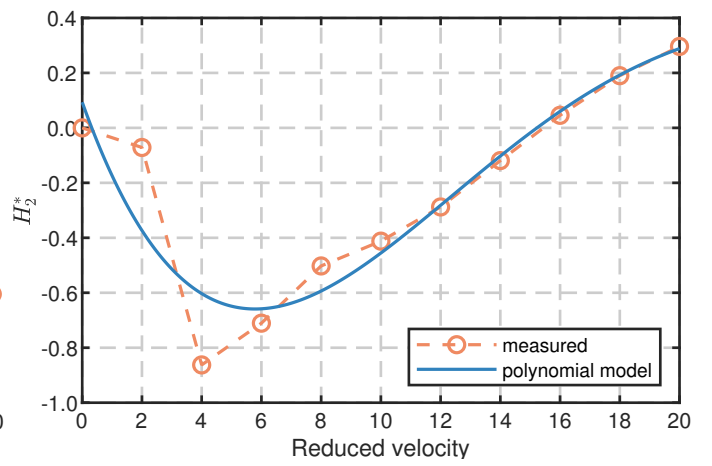
5 | DYNAMIC PROPERTIES

5.1 | Modal frequencies

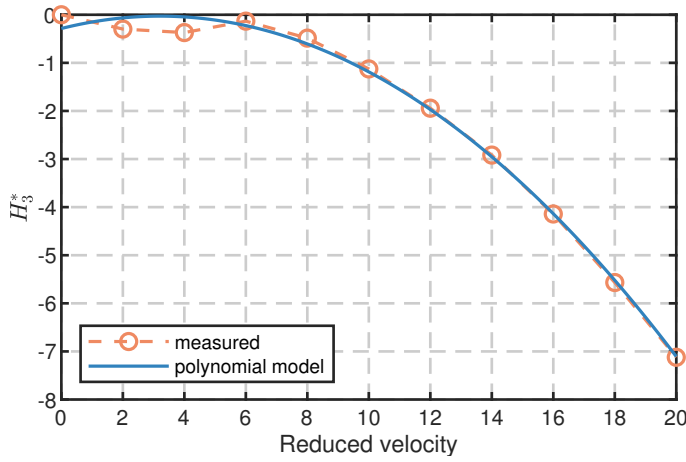
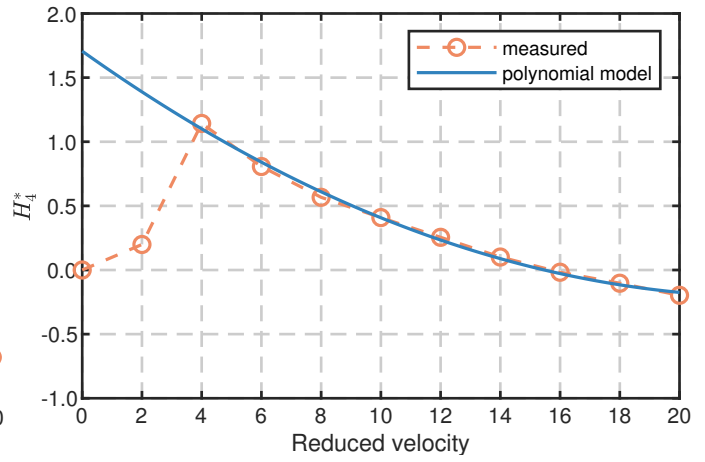
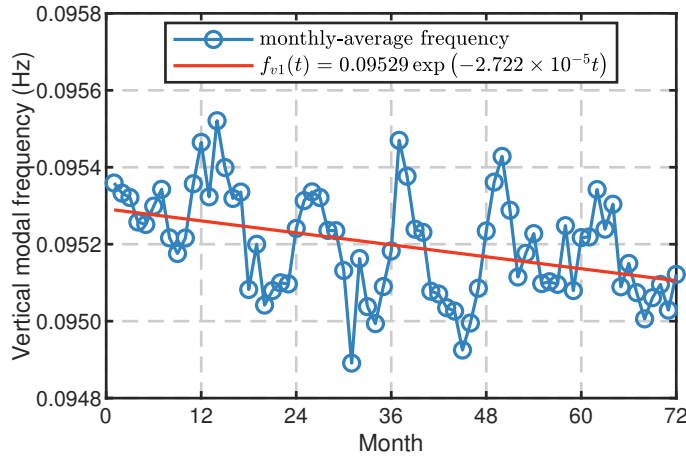
In this section, a solution is proposed to describe the time-variant structural properties, where the structural deterioration due to aging is modeled by a time-variant function and the fluctuation due to inter-seasonal environmental effects is described by probability distributions. In order to eliminate the unavoidable data recoding gaps of SHM, the MPVs of modal frequencies are averaged monthly in Fig. 8. The time-variant deterioration of modal frequencies is a function of time, unit of which is month. Meanwhile, probability distributions of the fluctuation can be obtained from regression residuals of the time-variant functions.

5.1.1 | Time-variant deterioration functions

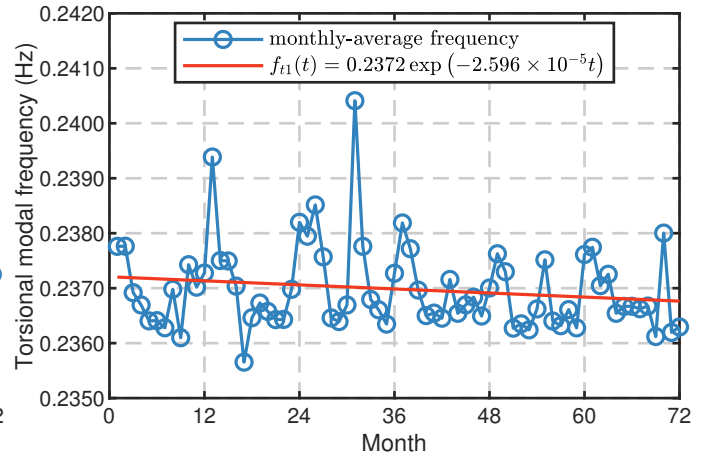
Fig. 8 presents the changing trends and variations of the monthly-averaged MPVs of modal frequencies. It shows obviously that the modal frequencies have been decreasing generally with time due to aging and fluctuating inter-seasonally. To quantitatively

(a) Flutter derivative A_1^* (b) Flutter derivative A_2^* (c) Flutter derivative A_3^* (d) Flutter derivative A_4^* (e) Flutter derivative H_1^* (f) Flutter derivative H_2^*

describe the time-variant deterioration, an exponential function $f(t) = a \exp(bt)$ is utilized to perform the regression analysis, where the unit of t is month. The time-variant deterioration functions fitted in Fig. 8 are based on historical data (2010-2015)

(g) Flutter derivative H_3^* (h) Flutter derivative H_4^* **FIGURE 7** Flutter derivatives of Xihoumen Bridge section model

(a) Monthly-averaged vertical modal frequency



(b) Monthly-averaged torsional modal frequency

FIGURE 8 1st-order asymmetric vertical and torsional modes: monthly-averaged modal frequencies and corresponding fitting curves

of the SHM system for Xihoumen Bridge. According to the deterioration functions, the predicted vertical modal frequency will decline from 0.09529 to 0.09223 in 100 years later, about 3.2%. Similarly, the predicted torsional modal frequency will decline from 0.2372 to 0.2299, about 3.1%.

5.1.2 | Probability distributions of inter-seasonal fluctuations

As shown in Fig. 8, the MPVs fluctuate inter-seasonally. The probability distributions of inter-seasonal fluctuations can be fitted by 72-month regression residuals. Normal distribution and generalized extreme value (GEV) distribution are utilized to describe these fluctuations. The PDF of Normal distribution with location parameter μ and scale parameter σ is

$$f(x|\mu, \sigma) = \frac{1}{\sqrt{2\pi}\sigma} \exp\left(-\frac{(x - \mu)^2}{2\sigma^2}\right) \quad (18)$$

The PDF of GEV distribution with location parameter μ , scale parameter σ , and shape parameter k ($k \neq 0$) is

$$f(x|k, \mu, \sigma) = \left(\frac{1}{\sigma}\right) \exp\left(-\left(1 + k\frac{(x - \mu)}{\sigma}\right)^{-\frac{1}{k}}\right) \left(1 + k\frac{(x - \mu)}{\sigma}\right)^{-1 - \frac{1}{k}} \quad (19)$$

Especially, Kolmogorov-Smirnov test (ks-test) is utilized to verify the goodness of the fitted probability distributions. The significance p -value is set as 0.05. Fig. 9 illustrates the fitted Normal distribution curves, GEV distribution curves and their corresponding ks-test values. For the 1st-order asymmetric vertical mode, Normal distribution and GEV distribution can both meet the requirement of ks-test with $p > 0.05$. For the 1st-order asymmetric torsional mode, only GEV distribution is qualified with $p = 0.53 > 0.05$, and Normal distribution is rejected with $p = 0.04 < 0.05$. In this study, GEV distributions are adopted for both modes.

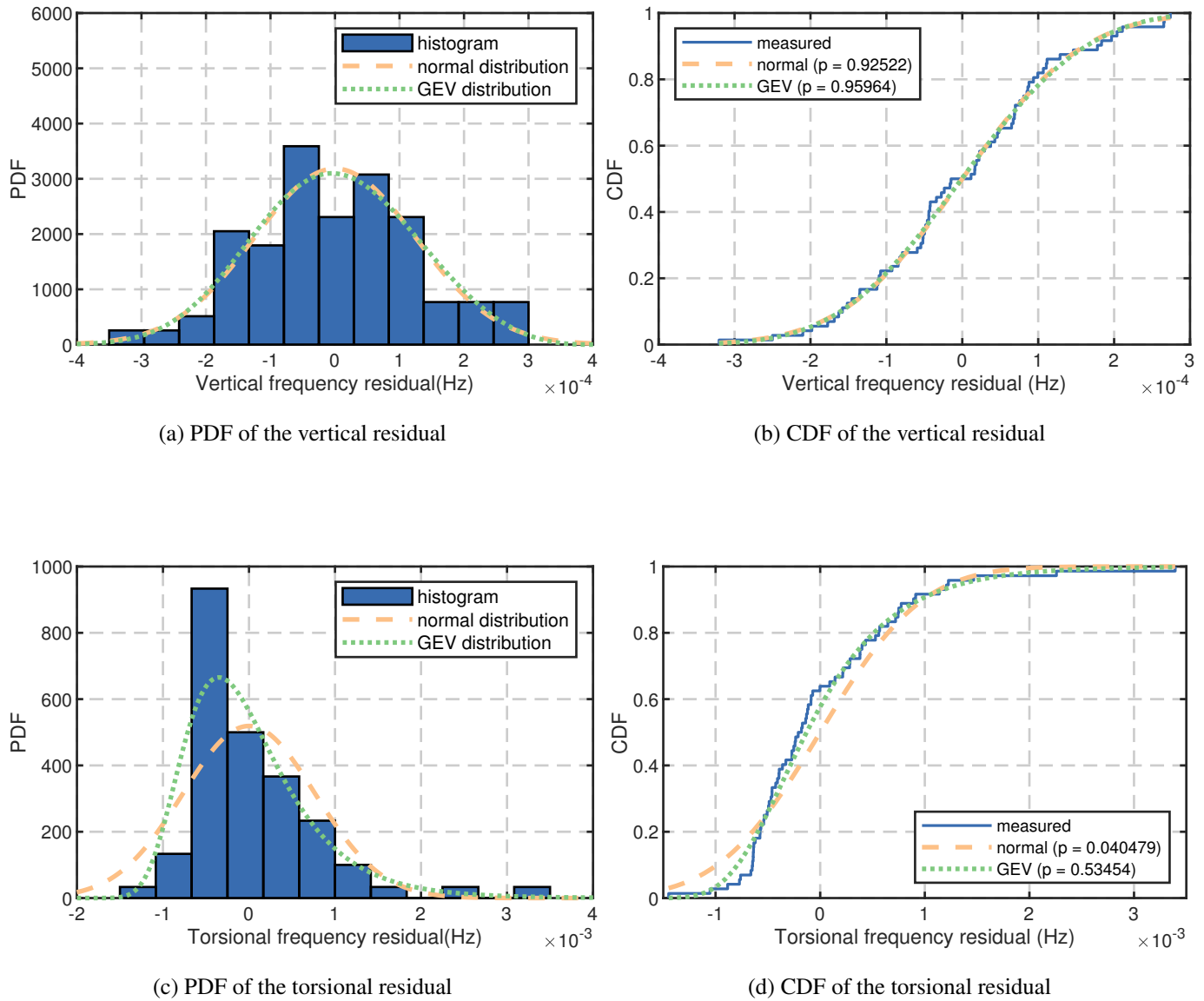
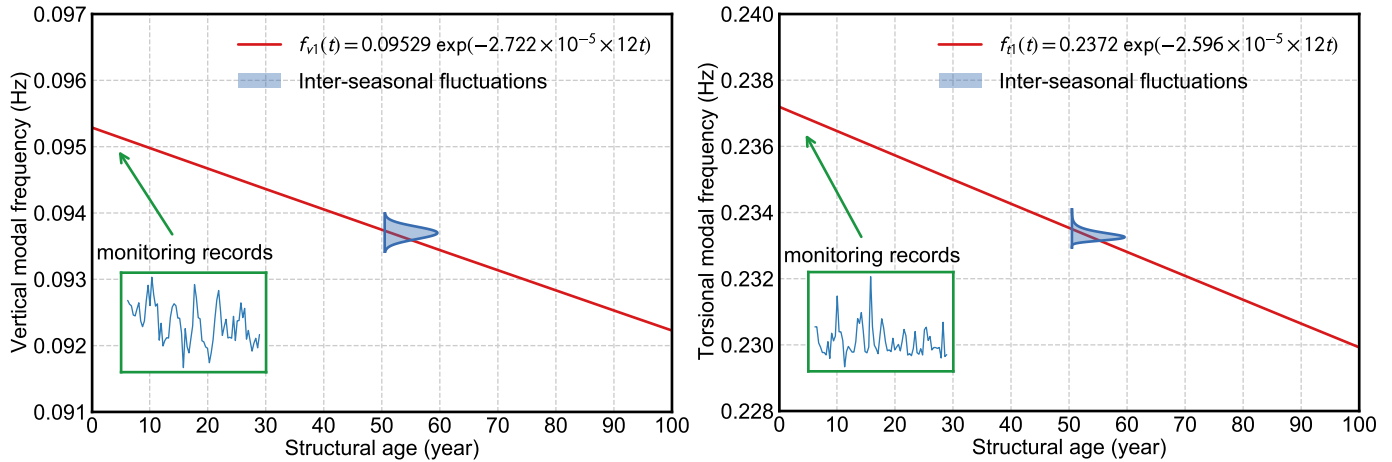


FIGURE 9 1st-order asymmetric vertical and torsional modes: PDF and CDF of inter-seasonal fluctuations of modal frequencies, fitted by 72-month regression residuals

5.1.3 | Long-term evolutions of modal frequencies

In Fig. 10, futuristic 100-year modal frequencies are predicted, based on first 6-year monitoring records. The unit of the x axis here is year rather than month, which leads to a modification of deterioration functions in terms of time t , as $f_{v1}(t)$ and $f_{t1}(t)$ in Fig. 10 show. In the long term, the modal frequencies can be described as the combination of a deterministic value (obtained by $f_{v1}(t)$ and $f_{t1}(t)$) and a random variable (blue areas of the inter-seasonal fluctuations), as illustrated in Fig. 10. In this study, the probability distribution of the inter-seasonal fluctuations are time-invariant inferred from Fig. 8, which prefigures that only mean values of modal frequencies' PDFs are changing with time, but standard variances of modal frequencies' PDFs are time-invariant. Modal frequencies' PDFs will not vary sharply from January to December of the same year. As a result in Sec. 6.1, the modal frequencies' PDFs in June of each year are chosen as the representative probability distributions to calculate the PDF of the flutter critical wind speed in that year.



(a) Evolution of 1st-order vertical modal frequency in 100-year structural age (b) Evolution of 1st-order torsional modal frequency in 100-year structural age

FIGURE 10 1st-order asymmetric vertical and torsional modes: prediction of modal frequencies in futuristic 100-year structural age, based on first 6-year monitoring records

5.2 | Damping ratios

MPVs of damping ratios are also averaged monthly, as presented in Fig. 11. Compared with modal frequencies, the long-term deterioration of damping ratios is ambiguous, but the inter-seasonal fluctuation is much more remarkable. Therefore, the long-term changing trend of damping ratios is negligible. Thus, only the inter-seasonal fluctuations are considered for damping ratios. Noticeably, with futuristic monitoring data, the deterioration effect of damping ratios might be more clear and non-negligible, which remains to be investigated further.

Lognormal distribution, Gamma distribution and GEV distribution are utilized to model the inter-seasonal fluctuations of damping ratios.

The PDF of Lognormal distribution is

$$f(x|\mu, \sigma) = \frac{1}{x\sigma\sqrt{2\pi}} \exp\left(-\frac{(\ln x - \mu)^2}{2\sigma^2}\right) \quad (20)$$

where μ and σ are the location parameter and scale parameter, respectively.

The PDF of Gamma distribution is

$$f(x|a, b) = \frac{1}{b^a\Gamma(a)} x^{a-1} e^{-\frac{x}{b}} \quad (21)$$

where $\Gamma(\cdot)$ is the Gamma function, a is a shape parameter, b is a scale parameter.

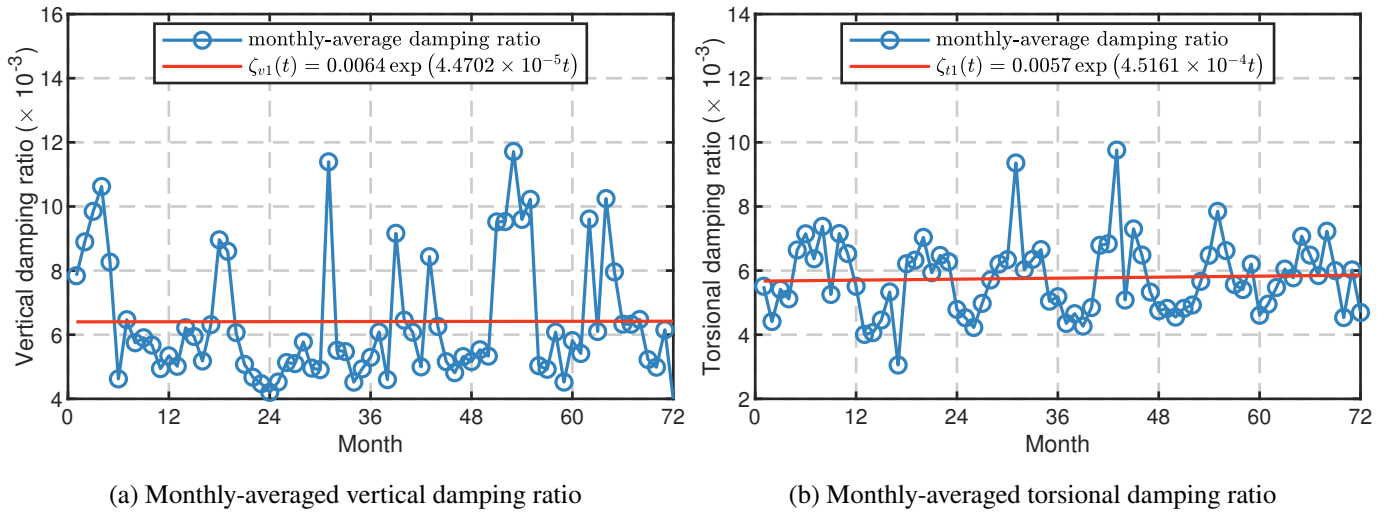
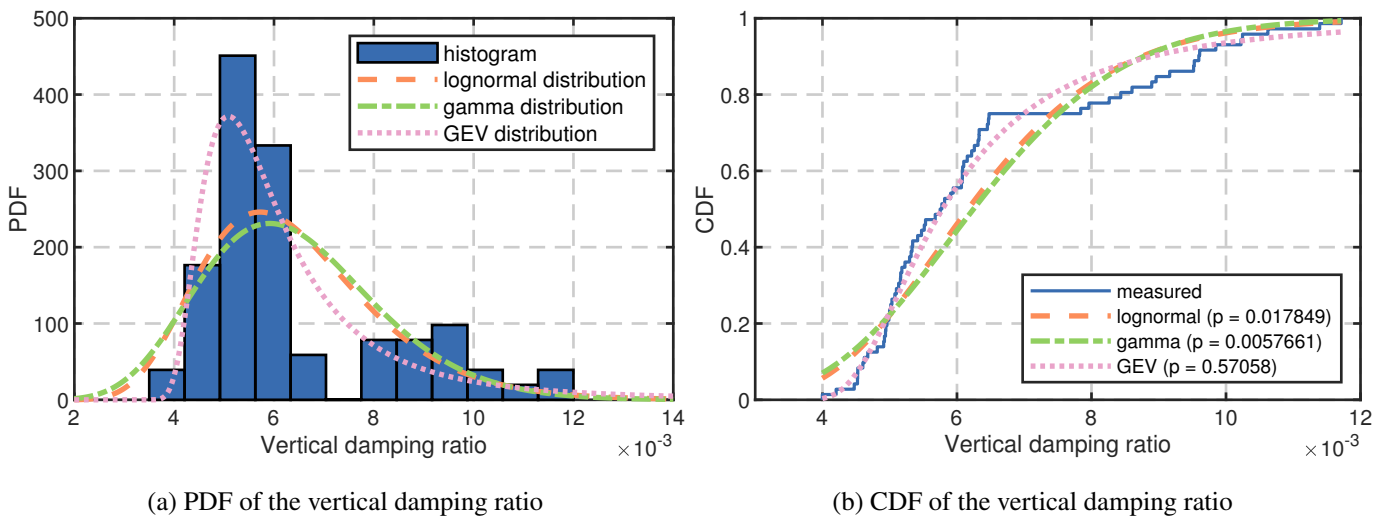


FIGURE 11 1st-order asymmetric vertical and torsional modes: monthly-averaged damping ratios and corresponding fitting curves

Fig. 12 illustrates the fitted distribution curves and their corresponding ks-test results. For 1st-order vertical mode, GEV distribution fits well with $p = 0.57 > 0.05$, yet Lognormal distribution and Gamma distribution are both rejected with $p < 0.05$. For 1st-order torsional mode, all three distributions fit well with $p > 0.05$. In this study, the distributions with largest p values are employed. Hence, GEV distribution and Gamma distribution are adopted to fit the inter-seasonal fluctuations of 1st-order vertical and torsional modes, respectively.

5.3 | Correlation of modal frequencies and damping ratios

In Fig. 13, the identified modal frequencies and damping ratios of 1st-order asymmetric vertical and torsional modes are plotted to verify their correlations, based on 6-year monitoring data. It shows that the correlation coefficients are -0.0191 and -0.0240, respectively for the vertical mode and torsional mode. Their correlations are not statistically significant. Thus for the same mode, the variance of the modal frequency is independent with the variance of the damping ratio, which leads to the assumption in Eq. (16) that the variances of f_i and ζ_i ($i = v1, t1$) are independent.



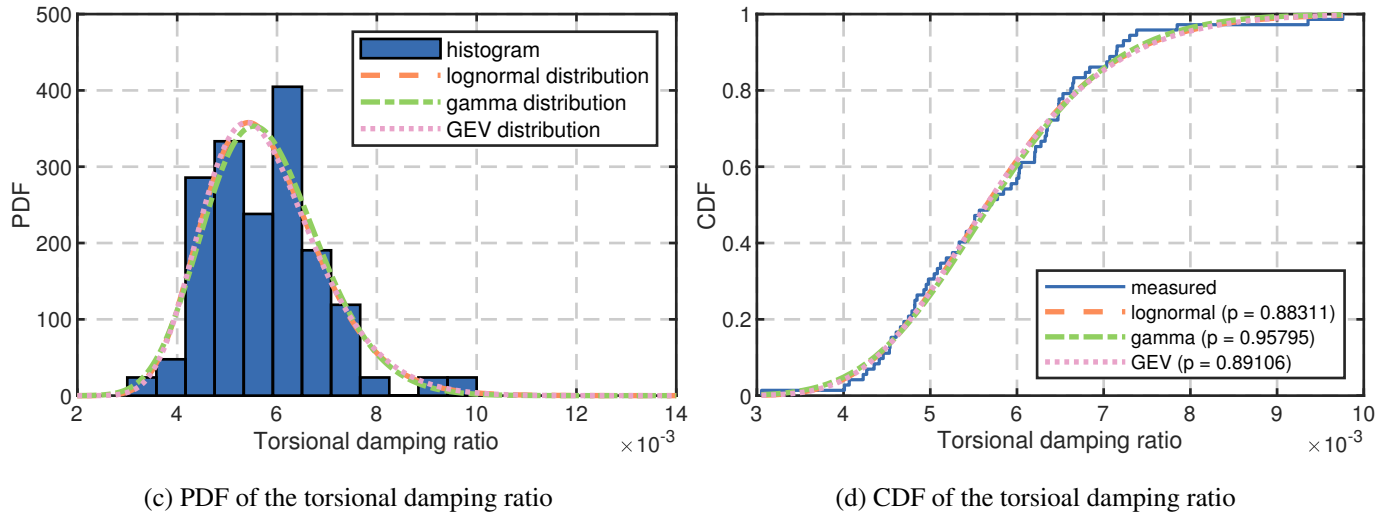


FIGURE 12 1st-order asymmetric vertical and torsional modes: PDF and CDF of monthly-averaged damping ratios

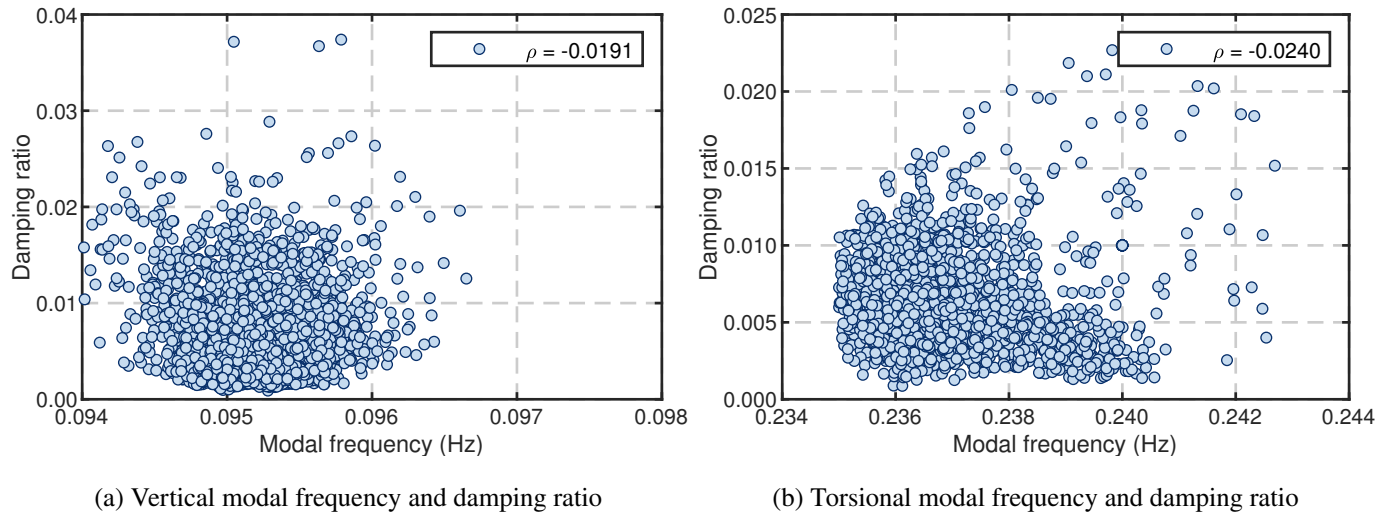


FIGURE 13 Correlations for modal frequencies and damping ratios of 1st-order asymmetric modes, based on first 6-year monitoring data

6 | NUMERICAL SIMULATION OF LIFE-CYCLE FLUTTER PROBABILITY

6.1 | Distribution of flutter critical wind speed

The flutter critical wind speed is calculated by the method suggested in Sec. 2.1. In order to incorporate the entire possible life-cycle structural properties, ranges of f_{v1} , f_{t1} , ζ_{v1} and ζ_{t1} are set as (0.090,0.100), (0.226,0.238), (0.004,0.012) and (0.003,0.010), respectively. Then the regression coefficients α_{v1} , α_{t1} , β_{v1} , β_{t1} and c in Eq. (16) can be obtained. The performance of the proposed linear regression model is good with $R^2 \approx 0.99$, as illustrated in Fig. 14.

Fig. 15 presents the distribution of the flutter critical wind speed at the beginning stage (structural age = 0), where the Eq. (16) is validated with the Monte-Carlo Simulation (MCS).

As shown in Fig. 16, the mean value of the flutter critical wind speed in the long term tends to decrease in the structural life cycle, due to the deterioration effects of modal frequencies. Since only the mean values of modal frequencies' PDFs are changing and the standard variances of modal frequencies' PDFs are time-invariant, the standard variance of the flutter critical wind speed PDF will also be time-invariant.

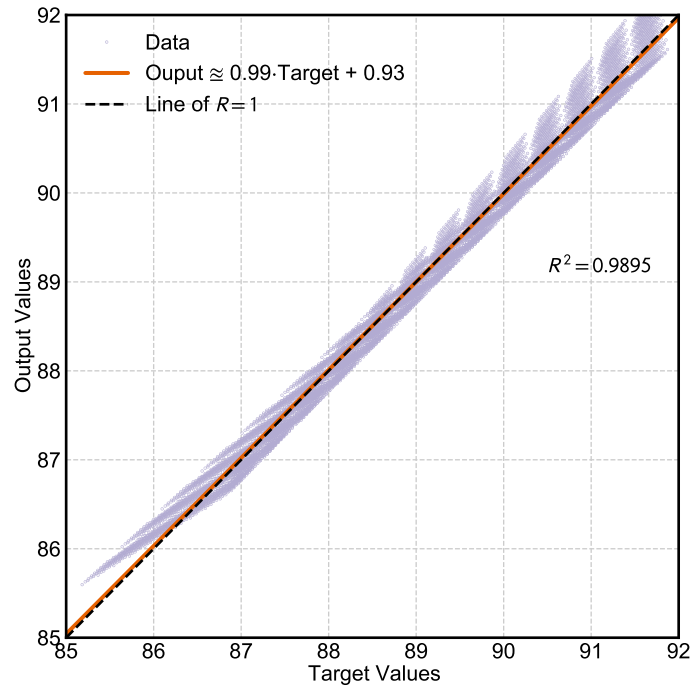


FIGURE 14 Performance of the proposed linear regression model between the flutter critical wind speed and 1st-order asymmetric modal properties

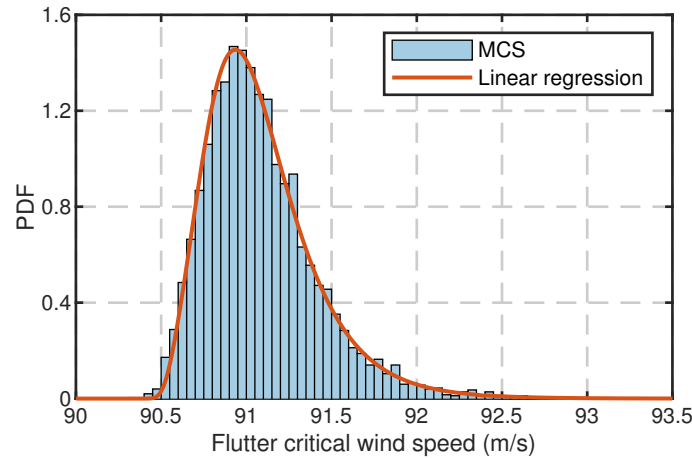


FIGURE 15 Validation of the proposed linear regression model with MCS: distribution of the flutter critical wind speed at the beginning stage

6.2 | Life-cycle flutter probability evolution due to deteriorations of modal properties

In this paper, the life-cycle flutter probability is calculated by Eq. (14). Due to the time-invariant PDFs of damping ratios, the long-term flutter probability in the futuristic 100 years caused by deteriorations of modal frequencies is presented in Fig. 17 with the label “no deterioration”, indicating that the failure probability might increase fairly fast with time, varying from 6.2×10^{-6} to 11.2×10^{-6} .

Due to the limitation of the monitoring period (only available from 2010-2015), however, the long-term deterioration effect of damping ratios is vague. The changing trends of damping ratios will be clearer with a longer monitoring period. In order to clarify the potential deterioration effects of damping ratios, it is assumed that the mean values of damping ratios will increase or decrease by 30% in 100 years later, rising or declining exponentially. The inter-seasonal fluctuations obey the same probability

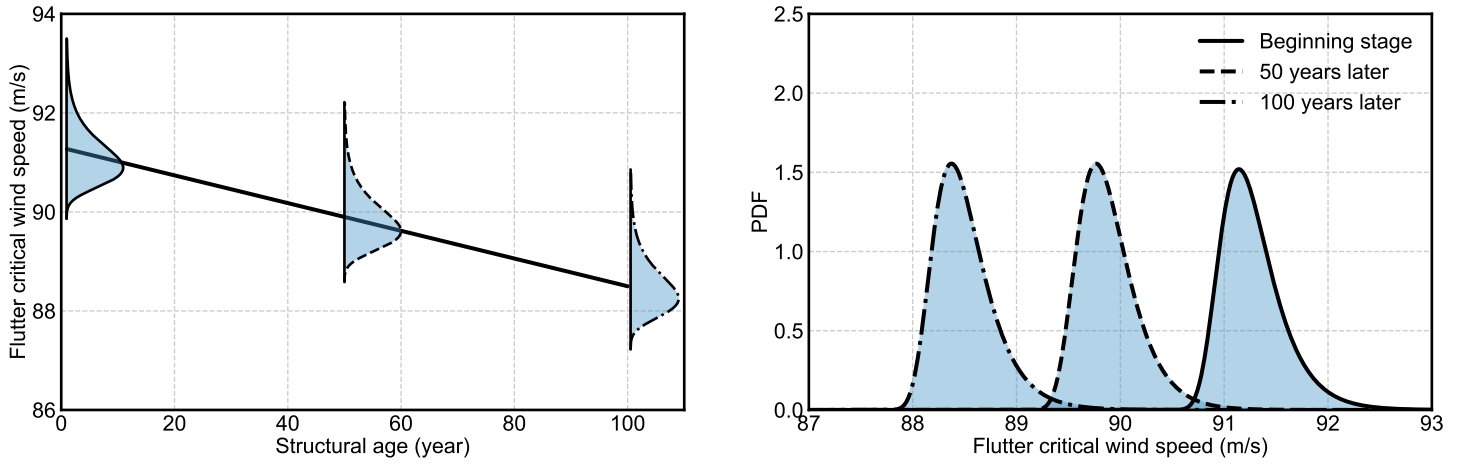


FIGURE 16 Distributions of the flutter critical wind speed in futuristic 100-year structural age

distributions mentioned in Sec 5.2. The long-term failure probability considering deterioration effects of modal frequencies and damping ratios simultaneously is illustrated in Fig. 17 with the labels “increase 30%” and “decrease 30%”.

As shown in Fig. 17, deteriorations of damping ratios rarely affect the failure probability, which is plausible because even 30% variation is still negligible compared with the inter-seasonal fluctuation. Therefore, it is suggested that more attention should be paid to the deteriorations of modal frequencies.

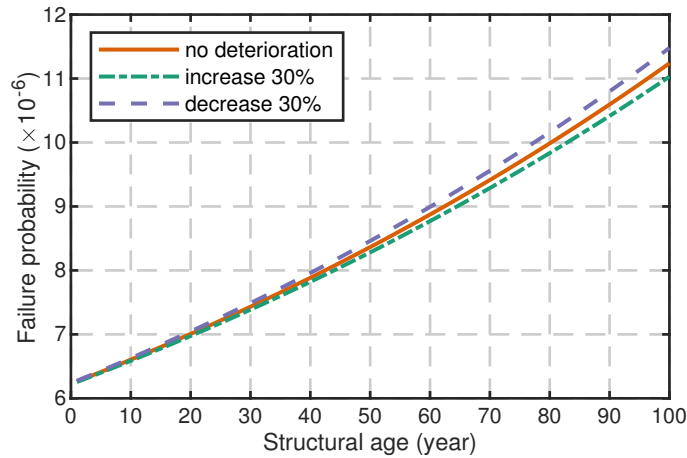


FIGURE 17 Comparison of various deterioration effects of damping ratios

7 | CONCLUSION

In this paper, an assessment methodology has been proposed to evaluate life-cycle flutter probability of long-span bridges based on field monitoring data. The 6-year dynamic properties including modal frequencies and damping ratios are extracted by the field monitoring data and the fast Bayesian approach, where the deterioration effects and inter-seasonal fluctuations are discussed in detail. Flutter critical wind speed is calculated by multi-mode flutter analysis based on the ideal structural model and the flutter derivatives identified by the wind tunnel test. A linear regression model is proposed to explicitly clarify how randomness is delivered from structural properties to the flutter critical wind speed, and to directly calculate the PDF of the flutter critical wind speed given the structural properties' PDFs. At last, the life-cycle flutter probability is calculated, considering the potential

deteriorations of modal frequencies and damping ratios. Based on the application example of Xihoumen Bridge, the flutter probability might increase fairly fast with deteriorations of modal frequencies, but nearly remain the same with deteriorations of damping ratios. This study shows that the structural deteriorations, which are usually neglected for the flutter analysis, should be considered for the flutter-resistance design.

ACKNOWLEDGMENTS

The authors gratefully acknowledge the support of National Natural Science Foundation of China (52008314, 51778495, 51978527, 52078383) and Shanghai Pujiang Program (No. 19PJ1409800). Any opinions, findings and conclusions or recommendations are those of the authors and do not necessarily reflect the reviews of the above agencies.

References

1. Theodorsen T. General theory of aerodynamic instability and the mechanism of flutter. 1949.
2. Jones NP, Scanlan RH. Theory and full-bridge modeling of wind response of cable-supported bridges. *Journal of Bridge Engineering* 2001; 6(6): 365–375.
3. Seo DW, Caracoglia L. Estimation of torsional-flutter probability in flexible bridges considering randomness in flutter derivatives. *Engineering structures* 2011; 33(8): 2284–2296.
4. Ji X, Huang G, Zhao YG. Probabilistic flutter analysis of bridge considering aerodynamic and structural parameter uncertainties. *Journal of Wind Engineering and Industrial Aerodynamics* 2020; 201: 104168.
5. Fang G, Cao J, Yang Y, Zhao L, Cao S, Ge Y. Experimental Uncertainty Quantification of Flutter Derivatives for a PK Section Girder and Its Application on Probabilistic Flutter Analysis. *Journal of Bridge Engineering* 2020; 25(7): 04020034.
6. Yang Y, Zhou R, Ge Y, Mohotti D, Mendis P. Aerodynamic instability performance of twin box girders for long-span bridges. *Journal of Wind Engineering and Industrial Aerodynamics* 2015; 145: 196–208.
7. Yang Y, Wu T, Ge Y, Kareem A. Aerodynamic stabilization mechanism of a twin box girder with various slot widths. *Journal of Bridge Engineering* 2015; 20(3): 04014067.
8. Caracoglia L. Simulation of linear and non-linear propagation effects of a random turbulence field on bridge flutter instability. *Journal of wind engineering and industrial aerodynamics* 2011; 99(9): 945–954.
9. Yang Y, Ge Y, Xiang H. Investigation on flutter mechanism of long-span bridges with 2d-3DOF method. *Wind and Structures* 2007; 10(5): 421–435.
10. Ni Y, Xia Y, Liao W, Ko J. Technology innovation in developing the structural health monitoring system for Guangzhou New TV Tower. *Structural Control and Health Monitoring* 2009; 16(1): 73–98.
11. Li S, Li H, Liu Y, Lan C, Zhou W, Ou J. SMC structural health monitoring benchmark problem using monitored data from an actual cable-stayed bridge. *Structural Control and Health Monitoring* 2014; 21(2): 156–172.
12. Katafygiotis LS, Yuen KV. Bayesian spectral density approach for modal updating using ambient data. *Earthquake engineering & structural dynamics* 2001; 30(8): 1103–1123.
13. Au SK. Fast Bayesian ambient modal identification in the frequency domain, Part I: Posterior most probable value. *Mechanical Systems and Signal Processing* 2012; 26: 60–75.
14. Au SK. Fast Bayesian ambient modal identification in the frequency domain, Part II: Posterior uncertainty. *Mechanical Systems and Signal Processing* 2012; 26: 76–90.
15. Ewins DJ. *Modal testing: theory and practice*. 15. Research studies press Letchworth . 1984.

16. Peeters B, De Roeck G. Stochastic system identification for operational modal analysis: a review. *J. Dyn. Sys., Meas., Control* 2001; 123(4): 659–667.
17. Brincker R, Zhang L, Andersen P. Modal identification of output-only systems using frequency domain decomposition. *Smart materials and structures* 2001; 10(3): 441.
18. Beck JL, Katafygiotis LS. Updating models and their uncertainties. I: Bayesian statistical framework. *Journal of Engineering Mechanics* 1998; 124(4): 455–461.
19. Beck JL. Bayesian system identification based on probability logic. *Structural Control and Health Monitoring* 2010; 17(7): 825–847.
20. Zhang FL, Ni YC, Lam HF. Bayesian structural model updating using ambient vibration data collected by multiple setups. *Structural Control and Health Monitoring* 2017; 24(12): e2023.
21. Yuen KV. *Bayesian methods for structural dynamics and civil engineering*. John Wiley & Sons . 2010.
22. Ciampoli M, Petrini F, Augusti G. Performance-based wind engineering: towards a general procedure. *Structural Safety* 2011; 33(6): 367–378.
23. Cui W, Caracoglia L. A unified framework for performance-based wind engineering of tall buildings in hurricane-prone regions based on lifetime intervention-cost estimation. *Structural Safety* 2018; 73: 75 - 86.
24. Spence SM, Kareem A. Performance-based design and optimization of uncertain wind-excited dynamic building systems. *Engineering Structures* 2014; 78: 133–144.
25. Seo DW, Caracoglia L. Exploring the impact of “climate change” on lifetime replacement costs for long-span bridges prone to torsional flutter. *Journal of Wind Engineering and Industrial Aerodynamics* 2015; 140: 1–9.
26. Ge Y, Xiang H, Tanaka H. Application of a reliability analysis model to bridge flutter under extreme winds. *Journal of Wind Engineering and Industrial Aerodynamics* 2000; 86(2-3): 155–167.
27. Prenninger P, Matsumoto M, Shiraishi N, Izumi C, Tsukiyama Y. Reliability of bridge structures under wind loading: consideration of uncertainties of wind load parameters. *Journal of Wind Engineering and Industrial Aerodynamics* 1990; 33(1-2): 385–394.
28. Ge Y, Tanaka H. Aerodynamic flutter analysis of cable-supported bridges by multi-mode and full-mode approaches. *Journal of Wind Engineering and Industrial Aerodynamics* 2000; 86(2-3): 123–153.
29. Mannini C, Bartoli G. Aerodynamic uncertainty propagation in bridge flutter analysis. *Structural Safety* 2015; 52: 29–39.
30. Cui W, Caracoglia L. Simulation and analysis of intervention costs due to wind-induced damage on tall buildings. *Engineering Structures* 2015; 87(0): 183 - 197.
31. Dragomirescu E, Miyata T, Yamada H, Katsuchi H. Probabilistic approach of structural reliability applied to bridge components. In: . 1. ; 2003: 789–796.
32. Cheng J, Cai C, Xiao Rc, Chen S. Flutter reliability analysis of suspension bridges. *Journal of Wind Engineering and Industrial Aerodynamics* 2005; 93(10): 757–775.
33. Rizzo F, Caracoglia L. Examination of experimental errors in Scanlan derivatives of a closed-box bridge deck. *Wind and Structures* 2018; 26(4): 231–251.
34. Rizzo F, Caracoglia L. Artificial Neural Network model to predict the flutter velocity of suspension bridges. *Computers & Structures* 2020; 233: 106236.
35. Pourzeynali S, Datta T. Reliability analysis of suspension bridges against flutter. *Journal of Sound and Vibration* 2002; 254(1): 143–162.

36. Canor T, Caracoglia L, Denoël V. Application of random eigenvalue analysis to assess bridge flutter probability. *Journal of Wind Engineering and Industrial Aerodynamics* 2015; 140: 79–86.
37. Petcherdchoo A, Neves LA, Frangopol DM. Optimizing lifetime condition and reliability of deteriorating structures with emphasis on bridges. *Journal of structural engineering* 2008; 134(4): 544–552.
38. Vu KAT, Stewart MG. Structural reliability of concrete bridges including improved chloride-induced corrosion models. *Structural safety* 2000; 22(4): 313–333.
39. Mori Y, Ellingwood BR. Reliability-based service-life assessment of aging concrete structures. *Journal of Structural Engineering* 1993; 119(5): 1600–1621.
40. Ellingwood BR, Lee JY. Life cycle performance goals for civil infrastructure: intergenerational risk-informed decisions. *Structure and Infrastructure Engineering* 2016; 12(7): 822–829.
41. Lee JY, Ellingwood BR. A decision model for intergenerational life-cycle risk assessment of civil infrastructure exposed to hurricanes under climate change. *Reliability Engineering & System Safety* 2017; 159: 100–107.
42. Alampalli S. Influence of in-service environment on modal parameters. In: . 1. Citeseer. ; 1998: 111–116.
43. Scanlan RH, Tomo J. Air foil and bridge deck flutter derivatives. *Journal of Soil Mechanics & Foundations Div* 1971.
44. Caracoglia L, Sarkar PP, Haan Jr FL, Sato H, Murakoshi J. Comparative and sensitivity study of flutter derivatives of selected bridge deck sections, Part 2: Implications on the aerodynamic stability of long-span bridges. *Engineering structures* 2009; 31(9): 2194–2202.
45. Yuen KV, Katafygiotis LS. Bayesian fast Fourier transform approach for modal updating using ambient data. *Advances in Structural Engineering* 2003; 6(2): 81–95.
46. Brownjohn JMW, Au SK, Zhu Y, et al. Bayesian operational modal analysis of Jiangyin Yangtze river bridge. *Mechanical Systems and Signal Processing* 2018; 110: 210–230.
47. Zhang FL, Au SK. Erratum for “Fast Bayesian FFT Method for Ambient Modal Identification with Separated Modes” by Siu-Kui Au. *Journal of Engineering Mechanics* 2013; 139(4): 545–545.
48. Frangopol DM, Lin KY, Estes AC. Life-cycle cost design of deteriorating structures. *Journal of Structural Engineering* 1997; 123(10): 1390–1401.
49. Chen A, Ma R, Wang D, Liu G, Ai H, Liu T. Wind-resistant design specification for highway bridges (in Chinese). *Ministry of Communications of the People's Republic of China: Beijing, China* 2018.
50. Cui W, Caracoglia L. Exploring hurricane wind speed along US Atlantic coast in warming climate and effects on predictions of structural damage and intervention costs. *Engineering Structures* 2016; 122: 209–225.
51. Melchers RE, Beck AT. *Structural reliability analysis and prediction*. John Wiley & Sons . 2018.
52. Li H, Laima S, Ou J, et al. Investigation of vortex-induced vibration of a suspension bridge with two separated steel box girders based on field measurements. *Engineering Structures* 2011; 33(6): 1894–1907.
53. Yang Y, Ma T, Ge Y. Evaluation on bridge dynamic properties and VIV performance based on wind tunnel test and field measurement. *Wind and Structures* 2015; 20(6): 719–737.
54. Zhang FL, Yang YP, Xiong HB, Yang JH, Yu Z. Structural health monitoring of a 250-m super-tall building and operational modal analysis using the fast Bayesian FFT method. *Structural Control and Health Monitoring* 2019; 26(8): e2383.
55. Li H, Li S, Ou J, Li H. Modal identification of bridges under varying environmental conditions: temperature and wind effects. *Structural Control and Health Monitoring* 2010; 17(5): 495–512.
56. Xia Y, Hao H, Zanardo G, Deeks A. Long term vibration monitoring of an RC slab: temperature and humidity effect. *Engineering structures* 2006; 28(3): 441–452.

57. Yuen KV, Kuok SC. Ambient interference in long-term monitoring of buildings. *Engineering Structures* 2010; 32(8): 2379–2386.
58. Zhao L, Cui W, Ge Y. Measurement, modeling and simulation of wind turbulence in typhoon outer region. *Journal of Wind Engineering and Industrial Aerodynamics* 2019; 195: 104021.

